Available online at www.sciencedirect.com

ScienceDirect

journal homepage: www.elsevier.com/locate/AJPS

Research Article

Targeted degradation of LRG1 to attenuate renal fibrosis

Linyao Fan[a,1], Yingqiu Qi[a,b,1], Xi Yang[a], Yarui Xu[a], Yana Zhang[a], Longdi Wang[a], Anying Zhu[c], Lirong Zhang[b], Jian Song[b], Shengnan Du[b,*], Guangjun Nie[d,*], Huan Min[a,b,*]

[a] *Henan Institute of Advanced Technology, Zhengzhou University, Zhengzhou 450003, China*
[b] *Department of Pharmacology, School of Basic Medical Sciences, Zhengzhou University, Zhengzhou 450001, China*
[c] *Academy of Medical Sciences, Zhengzhou University, Zhengzhou 450052, Henan, China*
[d] *CAS Key Laboratory for Biomedical Effects of Nanomaterials and Nanosafety & CAS Center for Excellence in Nanoscience, National Center for Nanoscience and Technology of China, 11 Beiyitiao, Zhongguancun, Beijing 100190, China*

ABSTRACT

Leucine-rich α-2 glycoprotein 1 (LRG1), a secreted glycoprotein, has been identified as significantly upregulated in renal fibrosis, potentially exacerbating the condition by enhancing TGF-β-Smad3-dependent signaling pathways. Herein, utilizing our developed LRG1-targeting peptide for LRG1 recruitment and lenalidomide for E3 ubiquitin ligase engagement, we developed an advanced proteolysis targeting chimera, ^{ET}TAC-2, specifically designed for LRG1 degradation. Our cellular degradation assays validated that ^{ET}TAC-2 effectively degraded LRG1 through a proteasome-dependent mechanism, achieving half-maximal degradation at a concentration of 8.38 µM. Furthermore, anti-fibrotic experiments conducted both *in vitro* and *in vivo* revealed that ^{ET}TAC-2 efficiently induced LRG1 degradation in fibrotic kidneys. This action effectively inhibited the TGF-β-Smad3 signaling pathway and diminished the secretion of fibrosis-associated proteins, consequently attenuating the progression of renal fibrosis. Our study highlights the pivotal role of LRG1 in renal fibrosis and positions ^{ET}TAC-2 as a promising therapeutic candidate for targeted LRG1 intervention.

1. Introduction

Renal fibrosis is the ultimate converging pathway for chronic kidney diseases and end-stage renal failure [1,2]. This disease is influenced by a myriad of etiological factors, including, but not limited to, bacterial infections, drug-related injuries, and complications arising from advanced diabetes [3–5]. Despite significant advances in understanding the molecular mechanisms underlying renal fibrosis, there

---

* Corresponding authors.
E-mail addresses: shengnandu@163.com (S. Du), niegj@nanoctr.cn (G. Nie), minh@zzu.edu.cn (H. Min).
[1] These authors contributed equally to this work.
Peer review under responsibility of Shenyang Pharmaceutical University.

remains a notable lack of efficacious therapeutic stratagems in clinical milieus [6–8]. The pivotal role of transforming growth factor-β (TGF-β) in initiating and advancing renal fibrosis has been thoroughly documented [9–11]. TGF-β influences various cellular processes by activating both the canonical Drosophila mothers against decapentaplegic (Smad)-dependent pathways and the noncanonical Smad-independent pathways [12–14]. The vigor and specificity of TGF-β signaling are finessed by several cellular receptors and secreted molecules, such as integrins, serine proteases, etc. [15–19]. These components interact with TGF-β and its receptors, either amplifying or mitigating TGF-β-mediated signaling pathways.

Leucine-rich α-2 glycoprotein 1 (LRG1) is a secreted glycoprotein belonging to the leucine-rich repeat protein family, which is believed to orchestrate the genesis and trajectory of a plethora of pathologies [20]. At the onset of renal fibrosis, a significant upregulation of LRG1 is observed in both the circulatory system and renal tissues [21]. Pioneering research led by Kyung Lee and colleagues demonstrated that increased LRG1 expression, particularly in the renal tubules of mice, exacerbates renal fibrosis caused by unilateral ureteral obstruction (UUO) [22]. In antithesis, the complete elimination of LRG1 substantially mitigated fibrosis triggered by both UUO and aristolochic acid exposure. Their further mechanistic investigations revealed that LRG1 accelerated renal fibrogenesis by facilitating the interaction between TGF-β and its receptors, leading to TGF-β-Smad3-dependent disease progression. These findings highlight LRG1 as a promising therapeutic target for renal fibrosis treatment.

Over the past decades, proteolysis-targeted chimeras (PROTACs) have emerged as a groundbreaking strategy in the field of protein degradation [23–26]. These chimeric molecules exploit the concept of molecular glues to connect E3 ubiquitin ligases with specific target proteins, facilitating their ubiquitination and subsequent proteasomal degradation. Structurally, a typical PROTAC comprises three essential components: a moiety that recruits the target protein, a flexible linker, and a moiety that engages an E3 ubiquitin ligase. One of the most notable features of PROTACs is their ability to degrade target proteins in a sub-stoichiometric fashion catalytically [27,28]. This mechanism holds the potential to reduce or delay the development of drug resistance, a significant challenge in current therapeutic approaches. Furthermore, since PROTACs operate by inducing proximity rather than necessitating occupancy at the target protein's active site, they offer a unique approach to modulating proteins previously considered "undruggable." This capability significantly expands the scope of therapeutic targets, paving the way for innovative approaches in drug discovery and development.

Recognizing the pivotal role of LRG1 in advancing renal fibrosis and the substantial superiority of PROTAC technology, this study focuses on developing a novel PROTAC for targeting LRG1 degradation. Utilizing our recently identified LRG1-targeting peptide (termed ET) as the domain for recruiting LRG1, and lenalidomide as the domain for recruiting the E3 ubiquitin ligase, we developed an optimized PROTAC (named [ET]TAC-2) through fine-tuning the linker length. Scheme 1 depicts the anti-fibrotic mechanism of [ET]TAC-2, which is specifically engineered to accumulate in fibrotic kidneys. Once there, it penetrates damaged renal cells to initiate the ubiquitination and subsequent degradation of LRG1. This intracellular degradation significantly reduces the extracellular secretion of LRG1, thereby attenuating the activation of the TGF-β-Smad3 signaling pathway, ultimately leading to a decrease in extracellular matrix secretion and effectively mitigating the progression of renal fibrosis. Both *in*
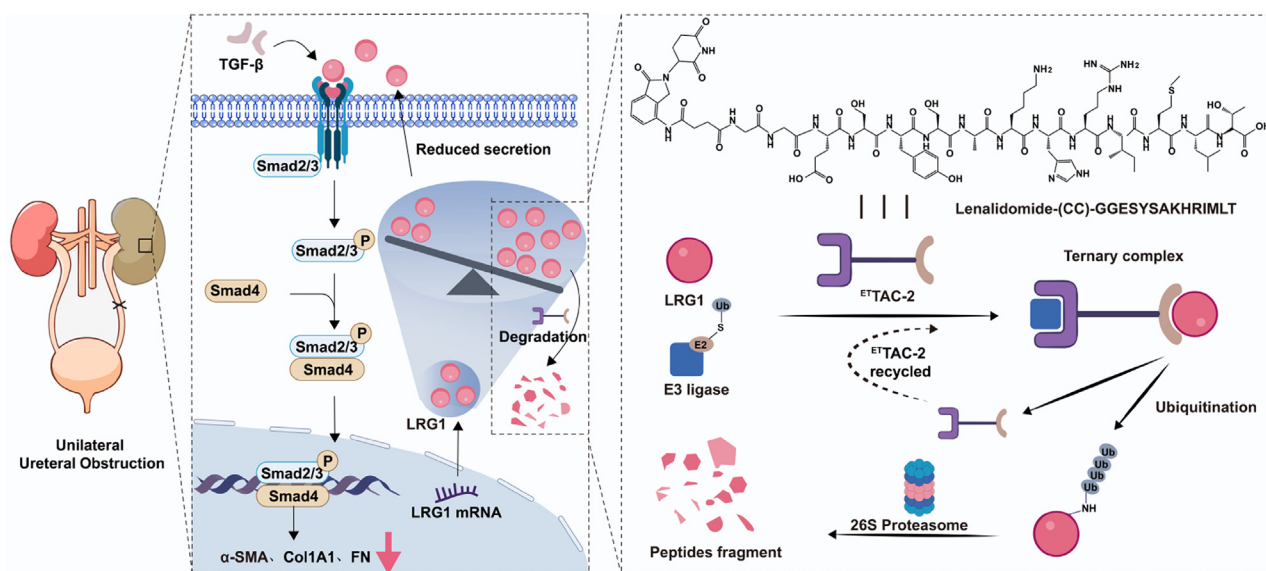
Scheme 1 – Schematic illustration of [ET]TAC-2 mediated anti-fibrosis via targeted LRG1 degradation. The prepared [ET]TAC-2, when administrated, preferentially accumulates in fibrotic kidneys and then penetrates damaged renal cells, initiating the ubiquitination and subsequent degradation of LRG1. This intracellular degradation process, induced by [ET]TAC-2, significantly diminishes the extracellular secretion of LRG1, thereby attenuating the activation of the TGF-β-Smad3 signaling pathway, ultimately leading to the decrease in extracellular matrix secretion and mitigating the progress of renal fibrosis.

vitro and *in vivo* therapeutic experiments have validated the efficiency of ^{ET}TAC-2 in degrading LRG1 within fibrotic kidneys and its efficacy in inhibiting the TGF-β-Smad3 pathway, thereby obstructing the progression of renal fibrosis. This research not only underscores the therapeutic potential of LRG1 in renal fibrosis but also pioneers a novel LRG1-targeting therapeutic agent, laying a solid groundwork for future advancements in LRG1-focused treatment approaches.

2. Materials and methods

2.1. Materials

The peptides ESYSAKHRIMLT (ET), MGHSHHMHRLNP (MP), and their Cy5-labeled counterparts, ET-Cy5 and MP-Cy5 (all with a purity of ≥95%), were procured from Guoping Pharmaceutical. The PBS, cell culture medium, and bicinchoninic acid (BCA) assay kit were obtained from Wuhan Service Biotechnology Co., Ltd. Fetal bovine serum (FBS) was purchased from Biological Industries. The AQP1 antibody was purchased from AMSBIO, while the LRG1 antibody was acquired from Santa Cruz Biotechnology. The α-SMA antibody, collagen 1A1 antibody and fibronectin antibody were supplied by Servicebio. The CRBN antibody was procured from Proteintech, and both the P-Smad3 antibody and Smad3 antibody were obtained from Affinity Biosciences. Hematoxylin, eosin, and the Cell Counting Kit-8 (CCK-8) were acquired from Solarbio Science & Technology Co., Ltd. The RNA primers were purchased from Hangzhou Sunya Biotechnology Co. LTD, and the sequences were listed as follows: mouse LRG1 (forward: 5'- TTGGCAGCATCAAGGAAGC -3', reverse: 5'-CAGATGGACAGTGTCGGCA -3'), Mouse 18S (forward, 5'-CGCCGCTAGAGGTGAAATTCT-3'; reverse, 5'- CGAACCTCCG ACTTTCGTTCT-3'); mouse α-SMA (forward, 5'-GTCCCAGACA TCAGGGAGTAA; TCGGATACTTCAGCGTCAGGA-3'); mouse collagen 1A1 (forward, 5'-GCTCCTCTTAGGGGCCACT; CCACGT CTCACCATTGGGG-3'); mouse fibronectin (forward, 5'-ATGT GGACCCCTCCTGATAGT; GCCCAGTGATTTCAGCAAAGG-3').

2.2. Synthesis of ^{ET}TACs and their characterization

Lenalidomide (CAS: 191732-72-6) was purchased from Bide Pharmatech Ltd. Unless otherwise noted, reagents and solvents were obtained from commercial suppliers and were used directly without further purification. Initially, we synthesize a series of lenalidomide derivatives that were modified with acid groups as follows:

Lenalidomide + **acids 1–4** $\xrightarrow[\text{DMF}]{\text{EDCI, HOBT}}$ **compounds 1–4**
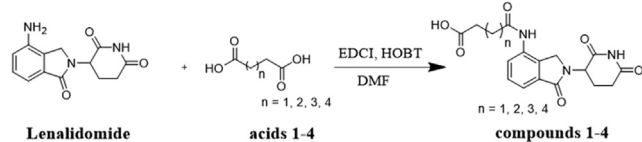
To a stirred solution of lenalidomide (1.0 mmol) in 12 ml DMF (N, N-Dimethylformamide) was added commercially available acids 1–4 (1.0 mmol), EDCI (N-(3-Dimethylaminopropyl)-N'-ethylcarbodiimide hydrochloride, 0.2 mmol) and HOBT (1-Hydroxybenzotriazole, 0.2 mmol). The reaction mixture was then stirred at 25 °C for 24 h. After that, water was added, and the mixture was extracted with ethyl acetate (three times). Then, the organic layers were combined, concentrated, and purified with flash column chromatography (dichloromethane/methanol =20:1 to 10:1, v/v) to obtain compounds 1~4.
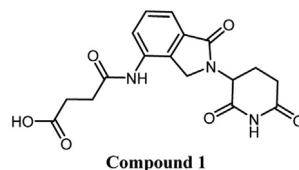
Compound 1

4-((2-(2,6-dioxopiperidin-3-yl)-1-oxoisoindolin-4-yl)amino)-4-oxobutanoic acid: Compound 1 was obtained from acid 1 according to general procedure. White solid; yield: 78.2 %; melt point: 172–174 °C. ^{1}H NMR (400 MHz, DMSO–d6) δ 12.18 (s, 1H), 11.04 (s, 1H), 9.88 (s, 1H), 7.83 (t, $J = 6.6$ Hz, 1H), 7.50 (d, $J = 6.9$ Hz, 2H), 5.18 – 5.12 (m, 1H), 4.35 (q, $J = 17.6$ Hz, 2H), 2.89 (s, 2H), 2.73 (s, 2H), 2.64 – 2.60 (m, 2H), 2.54 (t, $J = 6.2$ Hz, 2H). ^{13}C NMR (101 MHz, DMSO) δ 174.26, 173.30, 171.50, 170.83, 168.33, 134.25, 134.09, 133.15, 129.11, 125.56, 119.44, 52.04, 46.94, 31.68, 31.18, 29.50, 23.15. HRMS (ESI): *m/z* calcd for $C_{17}H_{17}N_3NaO_6$ (M + Na)$^+$, 382.1010, found, 382.1010. Purity 98.9 %.
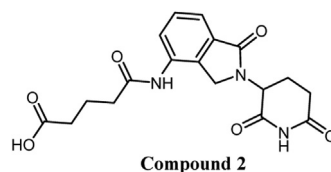
Compound 2

5-((2-(2,6-dioxopiperidin-3-yl)-1-oxoisoindolin-4-yl)amino)-5-oxopentanoic acid: Compound **2** was obtained from acid 2 according to general procedure. White solid; yield: 82.1%; melt point: 168–170 °C. ^{1}H NMR (400 MHz, DMSO) δ 12.01 (s, 1H), 11.01 (s, 1H), 9.78 (s, 1H), 7.85 – 7.79 (m, 1H), 7.50 (d, $J = 7.7$ Hz, 2H), 5.19 – 5.12 (m, 1H), 4.38 (s, 2H), 2.90 (d, $J = 7.7$ Hz, 2H), 2.37 (t, $J = 6.7$ Hz, 2H), 2.26 (t, $J = 6.8$ Hz, 2H), 1.68 – 1.53 (m, 4H). ^{13}C NMR (101 MHz, DMSO) δ 174.21, 173.30, 171.50, 170.79, 168.32, 134.24, 134.10, 133.15, 129.11, 125.57, 119.45, 52.04, 46.93, 31.69, 31.13, 29.44, 29.32, 23.16. HRMS (ESI): *m/z* calcd for $C_{18}H_{19}N_3NaO_6$ (M + Na) $^+$, 396.1166, found, 396.1167. Purity 99.4%.
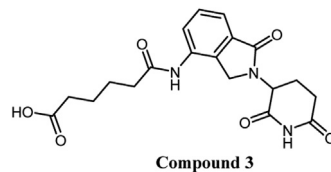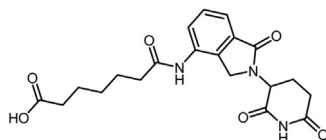
Compound 3

6-((2-(2,6-dioxopiperidin-3-yl)-1-oxoisoindolin-4-yl)amino)-6-oxohexanoic acid: Compound **3** was obtained from acid 3 according to general procedure. White solid; yield: 67.8%; melt point 154–156 °C; ^{1}H NMR (400 MHz, DMSO–d6) δ 12.01 (s, 1H), 11.01 (s, 1H), 9.78 (s, 1H), 7.81 (d, $J = 6.1$ Hz, 1H), 7.50 (d, $J = 7.7$ Hz, 2H), 5.18 – 5.12 (m, 1H), 4.38 (s, 2H), 2.89 (s, 2H), 2.38 (d, $J = 6.2$ Hz, 2H), 2.26 (t, $J = 6.8$ Hz, 2H), 2.04 (dd,

$J = 17.3$, 12.0 Hz, 2H), 1.66 – 1.50 (m, 4H).^{13}C NMR (101 MHz, DMSO–d6) δ 174.86, 173.34, 171.63, 171.54, 168.31, 134.23, 133.14, 129.10, 125.76, 119.49, 52.00, 46.94, 35.98, 33.90, 31.68, 25.10, 24.60, 23.09. HRMS (ESI): m/z calcd for $C_{19}H_{21}N_3NaO_6$ $(M + Na)^+$, 410.1323, found, 410.1324. Purity 92.1%.

Compound 4

7-((2-(2,6-dioxopiperidin-3-yl)-1-oxoisoindolin-4-yl)amino)-7-oxoheptanoic acid: Compound **4** was obtained from acid 4 according to general procedure. White solid; yield: 69.4%; melt point 142–144 °C; ^{1}H NMR (400 MHz, DMSO–d6) δ 11.00 (s, 1H), 9.75 (s, 1H), 7.82 (t, $J = 9.2$ Hz, 1H), 7.49 (d, $J = 7.1$ Hz, 2H), 5.20 – 5.07 (m, 1H), 4.36 (s, 2H), 2.89 (dd, $J = 29.8$, 17.2 Hz, 2H), 2.66 – 2.53 (m, 2H), 2.38 – 2.33 (m, 2H), 2.22 (t, $J = 7.1$ Hz, 2H), 1.57 (ddd, $J = 29.2$, 14.2, 7.0 Hz, 4H), 1.39 – 1.25 (m, 2H). ^{13}C NMR (100 MHz, DMSO–d6) δ 174.41, 172.82, 171.27, 171.03, 167.81, 133.77, 133.70, 132.64, 128.59, 125.24, 118.96, 51.51, 46.47, 35.63, 33.54, 31.17, 28.15, 24.78, 24.22, 22.59. MS (ESI) calculated for $C_{20}H_{23}N_3NaO_6$ $[M + Na]^+$ 424.1480, found 424.1480. Purity 98.7 %.

The raw ^{1}H NMR, ^{13}C NMR, mass spectrum, and HPLC elution spectra of these prepared four compounds are displayed in Figs. S12–S23. Subsequently, the four compounds obtained were used as special amino acids and coupled with the ET peptide through the classical solid-phase peptide synthesis method, resulting in the preparation of four [ET]TACs. The products were then purified using preparative-grade HPLC. The prepared [ET]TACs were characterized by HPLC and mass spectrum.

2.3. Cell culture and cellular fibrosis model

The human kidney proximal tubular epithelial cell line (HK-2) was cultured in Dulbecco's Modified Eagle Medium (DMEM) supplemented with 10% FBS and 1% penicillin-streptomycin under conditions of 37 °C and 5% CO_2. To establish a cellular model of fibrosis, HK-2 cells underwent a 24-h starvation period followed by treatment with 5 ng/ml transforming growth factor-beta (TGF-β) for an additional 24 h, the establishment of fibrosis model was verified by measuring the expression level of α-SMA with Western blot.

2.4. Flow cytometry and confocal microscopy detection of cellular uptake

HK-2 cells were seeded in a 6-well plate at a density of 3×10^5 cells per well. Post-adherence, the cells were treated with a medium containing 10 µM of either MP-Cy5 or ET-Cy5, followed by a 1-h- or 4-h-incubation period. Subsequently, the uptake was quantitatively assessed by flow cytometry. For confocal microscopy analysis, cells underwent the same treatment and were then fixed. The nuclei were stained with Hoechst 33342 (Beyotime), after which fluorescence images were captured using a confocal microscope.

2.5. Evaluation of LRG1 degradation in vitro

HK-2 cells were seeded in a 6-well plate at a density of 3×10^5 cells per well. Post-adherence, a starvation period of 6 h was implemented before drug treatment. (a) For the concentration-dependent LRG1 degradation assay, HK-2 cells received treatments of [ET]TAC-2, [ET]TAC-3, [ET]TAC-4, or [ET]TAC-5 at varying concentrations. Following a 12-h incubation period, the cells were harvested for protein analysis. (b) In the time-dependent LRG1 degradation experiment, HK-2 cells were exposed to [ET]TAC-2 for predetermined durations before protein analysis. (c) For the washout experiment, HK-2 cells, initially treated with [ET]TAC-2 for 12 h, underwent a medium change, were rinsed twice with PBS, and subsequently incubated in 10 % serum-containing medium for 0, 3, 6, 12, 24 and 48 h intervals before harvesting. (d) In the proteasome inhibition assay, cells were exposed to MG132, [ET]TAC-2, or their combination for 12 h. (e) The competitive inhibition assay involved treating cells with [ET]TAC-2, lenalidomide, free ET peptide, or their specific combinations for 12 h, followed by cell harvesting. The collected protein samples were determined with Western blot, employing GAPDH as an internal control to determine LRG1 expression levels.

2.6. Co-immunoprecipitation assay

HK-2 cells were exposed to either [ET]TAC-2 or PBS for 3 h. Post-treatment, cells underwent two PBS washes before lysis with 1.5 ml lysis buffer (Beyotime). To minimize non-specific protein binding, 20 µl Protein A/G PLUS-Agarose (Santa Cruz Biotechnology) was added to the cell lysates. A 100 µl sample of the lysate was reserved as an 'Input' control. The remaining lysate was equally divided for treatment with 2 µg either IgG (marked as IgG) or LRG1 antibody (marked as LRG1). Subsequently, 40 µl Protein A/G PLUS-Agarose was incorporated into each sample, followed by overnight incubation at 4 °C. The resulting precipitates were then collected. During the washing phase, samples were cleansed twice, first with Washing Solution I (1% Triton-X-100, 0.1% SDS, 150 mM NaCl) and then with Washing Solution II (1% Triton-X-100, 0.1% SDS, 50 mM HEPES). Prepared samples were processed for western blot analysis, employing GAPDH as an internal control to determine LRG1 expression levels.

2.7. Evaluation of [ET]TAC-2 induced anti-renal fibrosis in vitro

HK-2 cells were seeded in a 6-well plate at a density of 3×10^5 cells/well. The cellular fibrosis model was established as described above. Subsequently, the cells were treated with either PBS or [ET]TAC-2 for 12 h. Post-treatment, the cells were collected for further examination. qPCR was employed to assess the mRNA levels of α-SMA, collagen 1A1, and fibronectin following standardized procedures. Additionally, the protein levels of α-SMA, collagen 1A1, fibronectin, LRG1, t-Smad3, and P-Smad3 were analyzed using Western blotting, with GAPDH as the internal control. Protein grayscale values were quantified utilizing ImageJ software.

2.8. Animal model

Male C57BL/6 mice, weighing approximately 20 g each, were sourced from Sipeifu Biotechnology Co., Ltd., Beijing. These animal experiments were approved by the Animal Ethics Committee of Zhengzhou University, Zhengzhou, China (Ethics No. ZZUIRBGZR2023-1378). During the surgical process, mice were anesthetized with 1% pentobarbital sodium and positioned on their backs on a surgical table after shaving. An incision was made slightly to the right of the midline to reveal the ureter, identifiable by its tough, yellowish-white exterior. The ureter was carefully isolated, obstructed at both ends and cut in the middle. Subsequently, the incision was sutured. Animals underwent a 12-h fast before surgery but had access to water. The sham operation group underwent an identical procedure excluding the ureter obstruction. In the treatment group, mice received a 50 mg/kg intravenous dose of the therapeutic agent through the tail vein, commencing the day after the model was established. This regimen was maintained for five days, after which the mice were euthanized on Day 7 for therapeutic evaluation.

2.9. Blood circulation and biodistribution evaluation

To evaluate the *in vivo* blood circulation of -ET-Cy5, we intravenously injected either ET-Cy5 or MP-Cy5 into unilateral ureteral obstruction (UUO) mice, standardizing the doses to 7.5 mg/kg of Cy5 equivalent. The experimental groups were divided into UUO + MP-Cy5 and UUO + ET-Cy5. Blood samples were collected at pre-determined time points (0 h, 0.25 h, 0.5 h, 1 h, 2 h, 3 h, 5 h, 8 h, 12 h, 24 h) following administration, diluted with sodium heparin (10 mg/ml) at a 1:1 ratio, and analyzed using the IVIS imaging system for fluorescence imaging and semi-quantitative assessment.

To investigate ET-Cy5's renal targeting capability in UUO mice, we administered MP-Cy5, or ET-Cy5 (7.5 mg/kg of Cy5) intravenously to both sham-operated and UUO mice. The animals were divided into four groups: sham + MP-Cy5, Sham + ET-Cy5, UUO + MP-Cy5, and UUO + ET-Cy5. 6 h after injection, the mice were euthanized, and key organs (heart, liver, spleen, lungs, and kidneys) were harvested for ex vivo fluorescence imaging using the IVIS system. Kidney tissues were then rapidly frozen, prepared for histological examination, sectioned, and analyzed through IF staining.

2.10. Anti-fibrosis efficacy of ^ET^TAC-2 in vivo

Upon establishing the UUO model on Day 1, the animals were allocated into four groups: Sham, Sham + ^ET^TAC-2, UUO and UUO + ^ET^TAC-2, with five animals per group. From Day 2 to 6, ^ET^TAC-2 or saline with equivalent volume was administered daily at a dose of 50 mg/kg. The body weights of the mice were recorded throughout the experiment. On Day 7, the study concluded with the collection of blood serum and major organs, including the kidneys, heart, liver, spleen, and lungs, for subsequent analysis. Kidney tissues were imaged and weighed. For anti-fibrosis evaluation, qPCR was used to measure mRNA levels of α-SMA, collagen 1A1, and fibronectin in the kidney tissues, following standard procedures. Protein levels of α-SMA, collagen 1A1, fibronectin, LRG1, total Smad3,

and phosphorylated Smad3 were assessed via Western blot, using GAPDH as an internal control. Protein grayscale values were quantified using ImageJ software.

2.11. H&E staining and kidney injury scoring

Following the animal experiments, renal tissues were collected and subjected to hematoxylin and eosin (H&E) staining for histopathological analysis. The extent of kidney injury was assessed using H&E-stained images. Random fields were selected at $100\times$ magnification ($n = 5$) for injury evaluation, employing criteria such as tubular dilation, epithelial cell apoptosis, cast formation, and brush border loss. Injury severity was quantitatively scored on a scale from 0 to 4, with 0 indicating normal tissue, 1 for lesions affecting less than 25% of the field, 2 for lesions covering 25%−50%, 3 for those spanning 50%−75%, and 4 for lesions involving more than 75%.

2.12. Masson, IHC staining, and IF staining

Following the animal experiments, renal tissues were collected and subjected to Masson and IHC staining, which included markers such as α-SMA, collagen 1A1, fibronectin, and LRG1. Additionally, renal tissue sections underwent IF staining to assess the expression levels of P-Smad3 in the kidney tissue according to the operation manual.

2.13. Statistic analysis

All data are presented as mean $\pm$ SD (standard deviation) and were statistically analyzed using GraphPad Prism 8.0 software. Differences between the means of the two groups were assessed using the t-test. Significance levels are denoted as follows: $^*P < 0.05$; $^{**}P < 0.01$; $^{***}P < 0.001$.

3. Results and discussion

3.1. The analysis of LRG1 expression in UUO-induced renal fibrosis

The UUO is a well-recognized method for studying renal fibrosis in mice. As depicted in Fig. 1A, we established the UUO model via ligation of the unilateral ureter. Biochemical analyses of mouse serum, 7 d post-UUO, revealed marked renal dysfunction, as evidenced by elevated levels of blood urea nitrogen (BUN) and serum creatinine (SCR) (Fig. 1B and 1C). Subsequent histological examination of kidney tissues involved H&E staining, which demonstrated significant alterations in renal architecture, such as tubular dilation and epithelial cell detachment (Fig. 1D). These changes were quantitatively supported by pathological scoring (Fig. 1E). Immunohistochemical (IHC) staining for α-smooth muscle actin (α-SMA) indicated a pronounced increase in α-SMA expression in renal tissues post-UUO, confirming successful induction of renal fibrosis (Fig. 1F and 1G). Moreover, elevated LRG1 expression was observed post-UUO, with quantitative polymerase chain reaction (qPCR) analysis revealing a roughly 27-fold increase in LRG1 mRNA in kidneys (Fig. 1H), and IHC
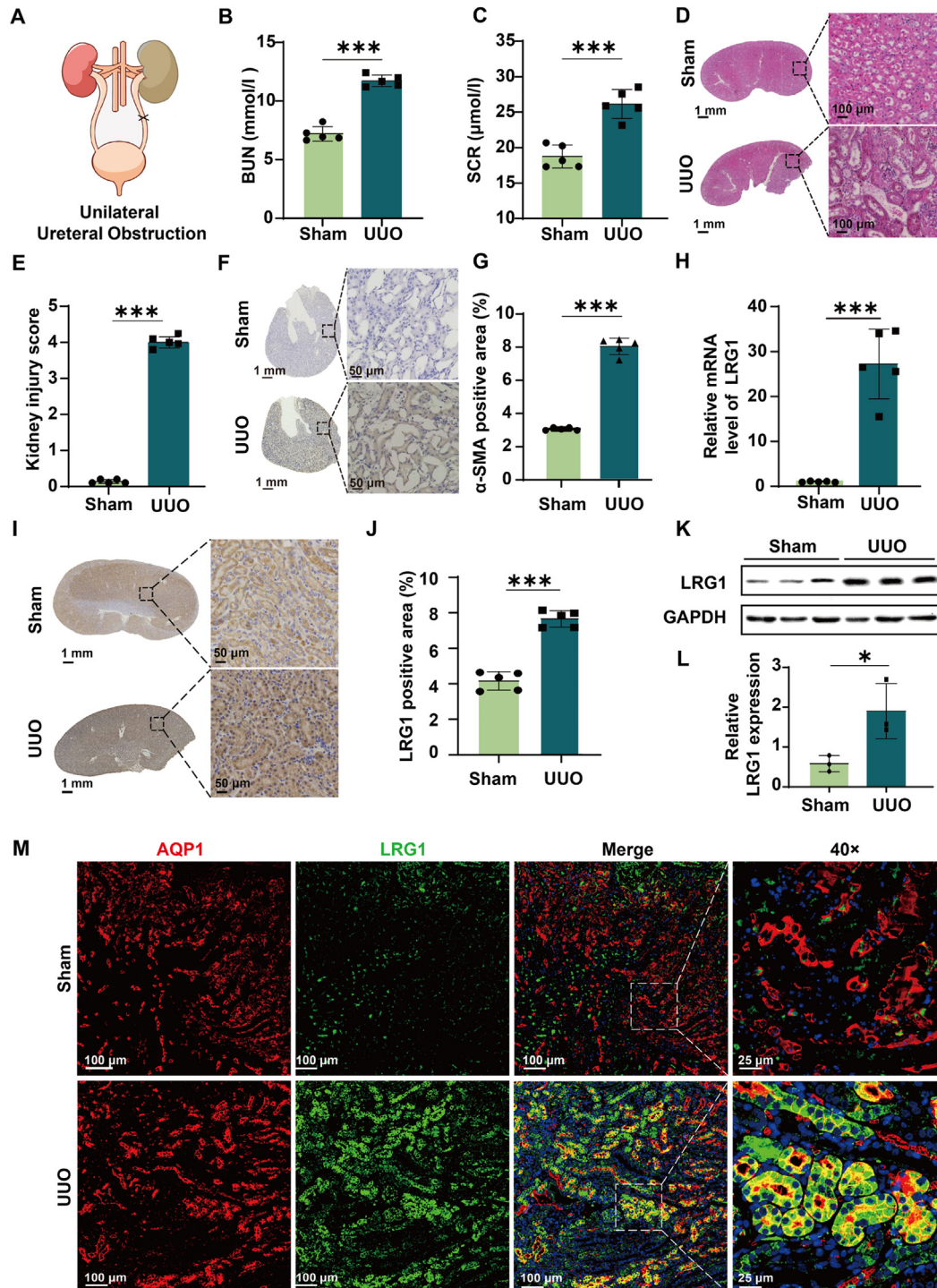
Fig. 1 – LRG1 is upregulated in UUO-induced renal fibrosis in mice. (A) The schematic illustration of the UUO model construction. (B) BUN and (C) SCR levels of mice 7 d post-UUO ($n = 5$). (D) H&E staining images and (E) corresponding kidney injury scores of kidney tissues ($n = 5$). (F) Immunohistochemical staining and (G) corresponding semi-quantitative analysis α-SMA in kidney tissues ($n = 5$). (H) Relative mRNA level of LRG1 in kidneys post-UUO ($n = 5$). (I) Immunohistochemical staining and (J) corresponding semi-quantitative analysis LRG1 of kidney tissues post-UUO ($n = 5$). (K) western blotting images and (L) corresponding quantitative analysis of LRG1 expressed in kidney tissues post-UUO ($n = 3$). (M) Representative immunofluorescence staining of kidney tissues post-UUO. LRG1 was stained in green. Aquaporin -1 (AQP1) (proximal tubular marker) was stained in red. Cell nuclei were stained in blue. Data are shown as mean ± SD; *$P < 0.05$; ***$P < 0.001$ when compared between indicated groups by two-way analysis of variance with a Tukey post hoc test.

staining confirming a substantial LRG1 increase (Fig. 1I and 1J). Western blot analysis further quantified this elevation, showing a more than 3-fold increase in LRG1 protein levels (Fig. 1K and 1L). Collectively, these data highlight a significant increase of LRG1 in kidneys post-UUO. To provide a detailed view of LRG1 localization post-UUO, immunofluorescence (IF) staining was performed on kidney sections, marking cell nuclei in blue, aquaporin-1 (AQP1) in red, and LRG1 in green. Fig. 1M displayed enhanced green fluorescence (LRG1) in post-UUO renal tissues, predominantly co-localizing with red fluorescence, suggesting that the upregulated LRG1 is primarily located near renal tubules.

3.2. ET peptide-mediated renal fibrosis targeting in vitro and in vivo

Based on the substantial upregulation of LRG1 in UUO-induced renal fibrosis in mice and its critical role in renal pathogenesis, LRG1 was supposed to be a promising therapeutic target for renal fibrosis. Our group has recently identified a peptide, named ET, that specifically targets LRG1 [29]. The ET peptide's targeting efficiency against LRG1-overexpressing breast tumors has been validated in both *in vitro* and *in vivo* studies. Thus, we propose that the ET peptide holds the potential for targeting renal fibrosis in mice by binding to LRG1. To validate this hypothesis, we labeled the ET peptide with cyanine dye Cy5 (ET-Cy5), alongside a Cy5 labeled control peptide (MP-Cy5), according to the reported method [29]. Besides, we established a cellular model of renal fibrosis and observed that TGF-β treatment significantly increased α-SMA expression in HK-2 cells, confirming the successful induction of cellular fibrosis (Fig. 2A and 2B). This treatment also elevated LRG1 expression in HK-2 cells (Fig. 2A and 2C), aligning with our previous findings in the UUO-induced renal fibrosis model. Using laser confocal scanning microscopy (LCSM) and flow cytometry, we assessed the *in vitro* targeting efficacy of the ET peptide for renal fibrosis. As shown in Fig. 2D, after a 4-h co-incubation, the red fluorescence in HK-2 cells treated with ET-Cy5 was markedly enhanced than in the MP-Cy5 treated cells. Furthermore, cells pre-treated with TGF-β exhibited a substantial increase in intracellular fluorescence compared to non-pre-treated cells. Quantitative flow cytometry analysis, as depicted in Fig. 2E and 2F, revealed that ET-Cy5 uptake by HK-2 cells was markedly enhanced than MP-Cy5, both with a 1-h and 4-h incubation. Remarkably, TGF-β pre-treated HK-2 cells showed a 3.6-fold and 4.6-fold increase in ET-Cy5 internalization efficiency after 1 h and 4 h, respectively, compared to untreated cells. The augmented fluorescence signal observed in cells subjected to ET-Cy5, in contrast to MP-Cy5, can be ascribed to the specific targeting ability of the ET peptide towards LRG1. Conversely, upon pre-treatment of cells with TGF-β, there is a notable elevation in LRG1 expression within cells, thereby amplifying the targeting efficacy of ET-Cy5. These findings collectively suggested that the ET peptide holds significant potential for targeting renal fibrosis effectively *in vitro*.

Building upon the confirmed affinity of ET peptide for renal fibrosis *in vitro*, we conducted a comprehensive assessment of its targeting capacity in a murine model of UUO-induced renal fibrosis. Blood clearance experiments in UUO mice revealed comparable elimination rates for both ET-Cy5 and MP-Cy5, as depicted in Figs. 2G and S1, with half-lives of 0.26 h and 0.17 h, respectively (Fig. 2H). After intravenous administrated with ET-Cy5 or MP-Cy5 to UUO and sham-operated mice, major organs were harvested six h post-injection for imaging analysis. As illustrated in Fig. 2I, 2J and S2, compared to the sham-operated groups or UUO mice treated with MP-Cy5, the fluorescence signal of Cy5 in mice injected with ET-Cy5 was predominantly localized in the obstructed kidney. Notably, even within the UUO mice, the fluorescence signal in the obstructed kidney was significantly higher than in the contralateral kidney. IF staining of kidney tissues post-imaging further confirmed ET-Cy5's targeting efficacy on fibrotic kidneys. As illustrated in Fig. 2K, the green LRG1 fluorescence signal was significantly more intense in the obstructed kidney compared to sham-operated ones, aligning with LRG1′s upregulation post-UUO. Additionally, the red fluorescence was substantially more pronounced in the obstructed kidney, exhibiting notable overlap with the green fluorescence of LRG1. These findings conclusively confirmed the targeting capacity of ET peptide against UUO-induced renal fibrosis *in vivo*, primarily attributable to its selective affinity for LRG1.

3.3. Evaluation of ^{ET}TAC-2 induced LRG1 degradation in vitro

Given the established affinity of the ET peptide for LRG1 and its effectiveness in targeting renal fibrosis *in vitro* and *in vivo*, we explored its potential as a basis for developing PROTACs specifically for LRG1 degradation. To explore this possibility, we used the ET peptide as the targeting moiety for LRG1 and lenalidomide as the ligand for the E3 ubiquitin ligase Cereblon (CRBN). By varying the linker length, we synthesized a series of PROTACs, named ^{ET}TACs. The molecular chemical structures and characterization profiles of these ^{ET}TACs, verified by high-performance liquid chromatography and mass spectrometry, are presented in Figs. S3–S6. Preliminary cytotoxicity evaluations, using cell counting kit-8, confirmed the good biocompatibility of these ^{ET}TACs at concentrations up to 100 µM (Fig. S7). Subsequent experiments revealed an obvious dose-dependent LRG1 degradation in HK-2 cells by all ^{ET}TACs, as illustrated in Figs. 3A and S8. The half-maximal degradation concentrations (DC$_{50}$) for ^{ET}TACs were determined as follows: ^{ET}TAC-2 at 8.38 µM, ^{ET}TAC-3 at 9.85 µM, ^{ET}TAC-4 at 13.23 µM, and ^{ET}TAC-5 at 24.6 µM, indicating the impact of linker length on their efficacy. Notably, ^{ET}TAC-2 emerged as the most potent in LRG1 degradation, meriting further exploration. Time-course studies, shown in Fig. 3B, confirmed that ^{ET}TAC-2 degraded LRG1 in a time-dependent manner. Furthermore, a washout assay indicated that LRG1 suppression persisted for 6 h post ^{ET}TAC-2 removal, with levels returning to normal after 12 h (Fig. 3C).

To ascertain that the observed LRG1 degradation was specifically induced by the synthesized ^{ET}TAC-2, not by its constituents, control degradation experiments were conducted with the ET peptide, lenalidomide, and their combination. As shown in Fig. S9, none of these treatments led to LRG1 degradation, thereby confirming the unique efficacy of ^{ET}TAC-2 in this process. Inhibition experiments
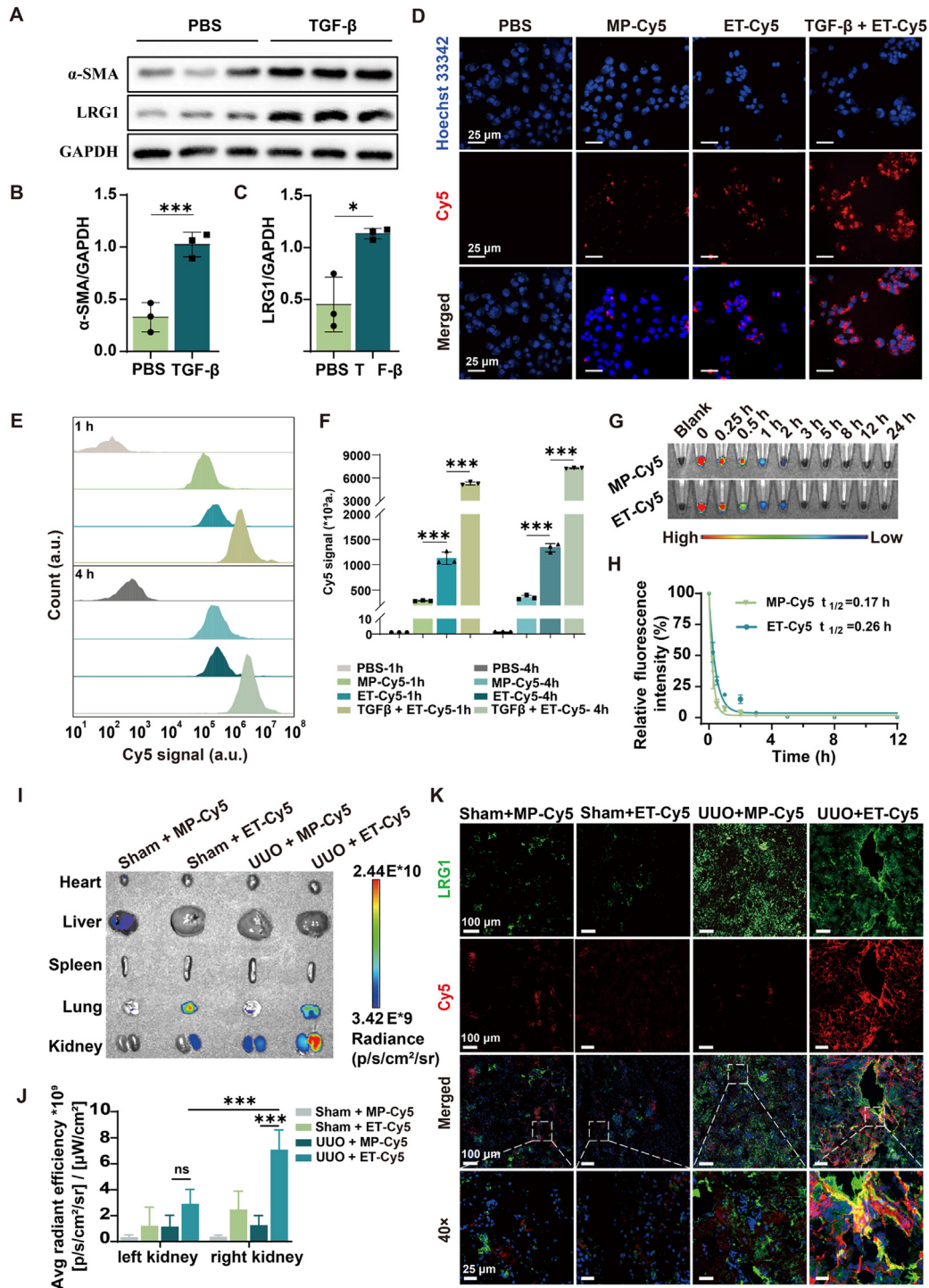
Fig. 2 – ET peptide targets renal fibrosis *in vitro* and *in vivo*. (A) Western blotting images and corresponding quantitative analysis of (B) α-SMA and (C) LRG1 in HK-2 cells treated with TGF-β ($n = 3$). (D) Representative confocal fluorescence images of HK-2 cells treated with MP-Cy5, ET-Cy5, or ET-Cy5 + TGF-β for 4 h. (E) Flow cytometry analysis and (F) corresponding quantitative analysis of HK-2 cells treated with MP-Cy5, ET-Cy5 or ET-Cy5 + TGF-β for 1 h or 4 h ($n = 3$). (G) Representative fluorescence images and (H) corresponding semi-quantitative analysis of blood samples collected at indicated time points from mice post-UUO ($n = 3$). (I) Representative fluorescence images of *ex vivo* major organs (including heart, liver, spleen, lung, and kidney) and (J) corresponding semi-quantitative analysis of average radiant efficiency of kidneys from mice treated with MP-Cy5 or ET-Cy5 ($n = 3$). (K) Fluorescence images of kidney sections derived from mice with different treatments. Cell nuclei were stained in blue and LRG1 was stained in green. Data are shown as mean ± SD; *$P < 0.05$; ***$P < 0.001$; ns, no significance, $P > 0.05$ when compared between indicated groups by two-way analysis of variance with a Tukey post hoc test.
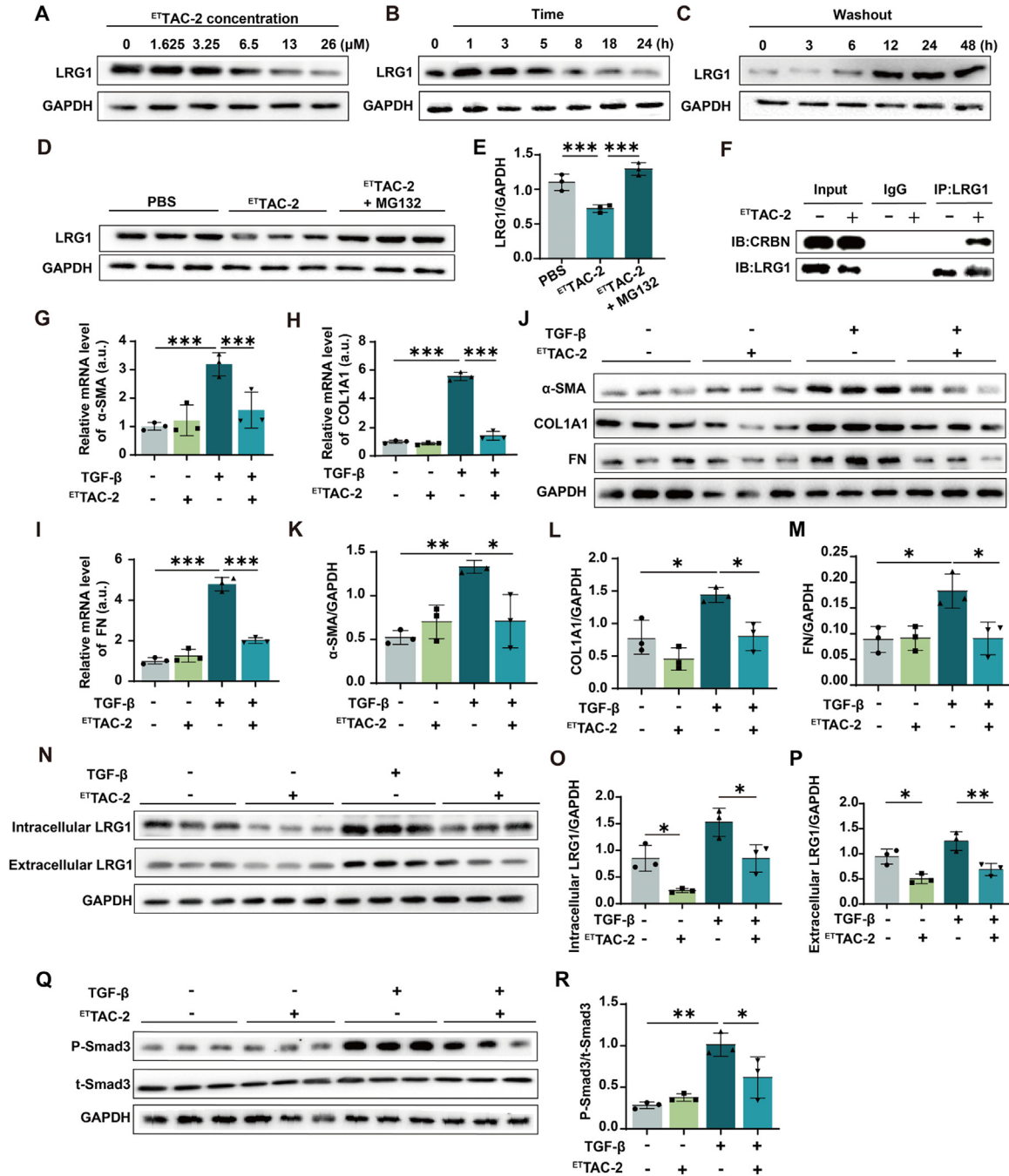
Fig. 3 – Evaluation of LRG1 degradation and anti-fibrosis effect induced by ^{ET}TAC-2 *in vitro*. Western blot images of LRG1 expression in HK-2 cells treated with (A) various concentrations of ^{ET}TAC-2 for 12 h and (B) ^{ET}TAC-2 of 8.38 µM for various incubation times. (C) Western blot images of LRG1 expressed in HK-2 cells after being treated with ^{ET}TAC-2 for 12 h and then replaced with fresh medium various times. (D) Western blot images and (E) corresponding quantitative analysis of LRG1 expression in HK-2 cells treated with either ^{ET}TAC-2 alone or a combination of ^{ET}TAC-2 and MG132, with both treatments at equivalent doses of ^{ET}TAC-2. $n = 3$ Per group. (F) Representative images of the co-immunoprecipitation experiment detected an interaction of ^{ET}TAC-2 with CRBN and LRG1. Relative mRNA level of (G) α-SMA, (H) collagen1A1, and (I) fibronectin in HK-2 cells with different treatments ($n = 3$). (J) Western blot images and (K-M) corresponding quantitative analysis of α-SMA, collagen1A1, and fibronectin in HK-2 cells with different treatments ($n = 3$). (N) Western blot images and (O-P) corresponding quantitative analysis of intracellular and extracellular LRG1 in HK-2 cells with different treatments ($n = 3$). (Q) Western blot images and (R) corresponding quantitative analysis of phosphorylated-Smad3 (p-Smad3) and total-Smad3 (t-Smad3) in HK-2 cells with different treatments ($n = 3$). Data are shown as mean ± SD; $*P < 0.05$; $**P < 0.01$; $***P < 0.001$ when compared between indicated groups by two-way analysis of variance with a Tukey post hoc test.

with MG132, a well-known proteasome inhibitor, as shown in Fig. 3D and 3E, provided evidence that ^{ET}TAC-2-induced LRG1 degradation relies on the proteasome system. Moreover, co-immunoprecipitation assays, depicted in Fig. 3F, verified the formation of a ternary complex involving CRBN, LRG1, and ^{ET}TAC-2, thus establishing that ^{ET}TAC-2 induced LRG1 degradation through the ubiquitin-proteasome pathway.

By optimizing the linker length, we developed ^{ET}TAC-2, which effectively degraded LRG1 with a DC_{50} of 8.38 µM and demonstrated a maximum degradation efficiency above 70 %. Nonetheless, the efficacy of ^{ET}TAC-2 was partially constrained by its substantial molecular weight and hydrophilicity, which may limit cellular uptake and endosomal escape. Enhancing these aspects through the integration of an ionizable tertiary amine or a cell-penetrating peptide into the linker might improve the LRG1 degradation efficiency of ^{ET}TAC-2. In summary, our developed ^{ET}TAC-2 demonstrated effective and selective LRG1 degradation via the ubiquitin-proteasome system.

3.4. ^{ET}TAC-2 alleviates cellular fibrosis in vitro by inhibiting the TGF-β-Smad3 pathway

Recognizing the pivotal role of LRG1 in promoting renal fibrosis and the exceptional efficacy of ^{ET}TAC-2 in LRG1 degradation, we explored the therapeutic potential of ^{ET}TAC-2 against renal fibrosis in vitro. As illustrated in Fig. 3G-3I, the results of qPCR revealed that TGF-β treatment significantly increased the transcription level of fibrotic marker proteins (including α-SMA, collagen-1A1, and fibronectin) in HK-2 cells. Remarkably, ^{ET}TAC-2 administration reduced the transcription levels of these proteins by 50.5%, 74.3% and 58%, respectively. Furthermore, Western blot analysis, presented in Fig. 3J–3M, demonstrated that ^{ET}TAC-2 significantly decreased the expression of α-SMA, collagen-1A1, and fibronectin by 46.7%, 44.3% and 50.4%, respectively, compared to TGF-β treatment alone. These findings, through qPCR and Western blot analysis, collectively underscore the anti-fibrotic efficacy of ^{ET}TAC-2 in vitro.

Further investigations delved into the underlying mechanism of ^{ET}TAC-2-mediated anti-fibrosis. As illustrated in Fig. 3N–3P, in HK-2 cells stimulated by TGF-β, ^{ET}TAC-2 treatment leads to a decrease in LRG1 expression, with a reduction of 44.4% intracellularly and 45.2% in its secretion into the culture medium. Recognizing LRG1's role in promoting renal fibrosis via the TGF-β-Smad3 pathway, we examined the pathway's activation level. As shown in Fig. 3Q–3R, ^{ET}TAC-2 treatment significantly decreased the phosphorylation levels of Smad3 by 38.9%, in TGF-β-induced fibrotic HK-2 cells. These findings collectively indicated that ^{ET}TAC-2 primarily hindered renal cellular fibrosis by reducing LRG1 expression, consequently suppressing the TGF-β-Smad3 pathway.

3.5. ^{ET}TAC-2 protects renal function in mice with renal fibrosis

Extending from the promising fibrosis inhibition observed in vitro, we further evaluated the therapeutic potential of ^{ET}TAC-2 against renal fibrosis in a UUO mouse model. As

depicted in Fig. 4A, mice post-UUO were administered with ^{ET}TAC-2 at 50 mg/kg daily for five d. Subsequent blood and renal tissue analysis post-treatment assessed the anti-fibrotic effectiveness of ^{ET}TAC-2. Serum biochemical assays indicated significant reductions in BUN and SCR levels in the ^{ET}TAC-2 group, implying effective mitigation of UUO-induced renal impairment (Fig. 4B and 4C). Ex vivo kidney inspections revealed that, compared to the sham and non-obstructed contralateral kidneys, the obstructed kidneys exhibited a paler appearance. However, ^{ET}TAC-2-treated mice displayed similar kidney appearances, with no notable differences (Fig. 4D). The analysis of the ratio of kidney weight to body weight demonstrated that ^{ET}TAC-2 treatment effectively reduced the weight increase of the obstructed kidney by 16.6%, as shown in Fig. 4E. Histopathological examination using H&E staining indicated that ^{ET}TAC-2 markedly decreased renal tubular dilatation and vacuolization in tubular epithelial cells caused by UUO (Fig. 4F). Additionally, renal tissue pathology injury scores revealed approximately a 50% reduction in renal pathological damage with ^{ET}TAC-2 treatment (Fig. 4G). These results collectively demonstrated the efficacy of ^{ET}TAC-2 in preserving renal tissue structure and function in UUO-induced renal fibrosis in mice.

3.6. ^{ET}TAC-2 alleviates renal fibrosis in vivo

Apart from assessing the protective effects of ^{ET}TAC-2 on renal function in mice with UUO-induced renal fibrosis, we further evaluated its anti-fibrotic efficacy. As shown in Fig. 5A and 5B, Masson trichrome staining revealed a 64.3% reduction in matrix deposition in the kidneys of ^{ET}TAC-2-treated UUO mice compared to their untreated counterparts. To quantitatively evaluate ^{ET}TAC-2's efficacy against renal fibrosis in vivo, we analyzed the expression of fibrotic marker proteins post-treatment. In UUO mice, the mRNA expression levels of α-SMA, collagen-1A1, and fibronectin were significantly elevated under untreated conditions compared to the sham group. However, these levels decreased by 79.4%, 74.2% and 58%, respectively, after treatment with ^{ET}TAC-2 (Fig. 5C–5E). IHC staining analysis further supported these results. In kidney sections from mice post-UUO, the expression areas of α-SMA, collagen-1A1, and fibronectin, which had significantly increased, were diminished by 64.4%, 73.4%, and 71.9%, respectively, following ^{ET}TAC-2's treatment (Fig. 5F-5K). Western blot analysis further quantified these changes, showing decreases in α-SMA, collagen-1A1, and fibronectin expression by 60.3%, 61.6% and 53.3%, respectively, in UUO mice after treatment of ^{ET}TAC-2 (Fig. 5L-5O). These collective results robustly confirmed the efficacy of ^{ET}TAC-2 in mitigating UUO-induced renal fibrosis in mice.

3.7. ^{ET}TAC-2 degrades LRG1 to inhibit the TGF-β-Smad3 pathway in vivo

Our study provided cellular-level evidence that ^{ET}TAC-2 potentially alleviated renal fibrosis by degrading LRG1, consequently inhibiting the TGF-β-Smad3 signaling pathway. To substantiate this hypothesis, we extended our investigations to mouse kidney tissues. IHC analyses, as illustrated in Fig. 6A and 6B, revealed a marked elevation
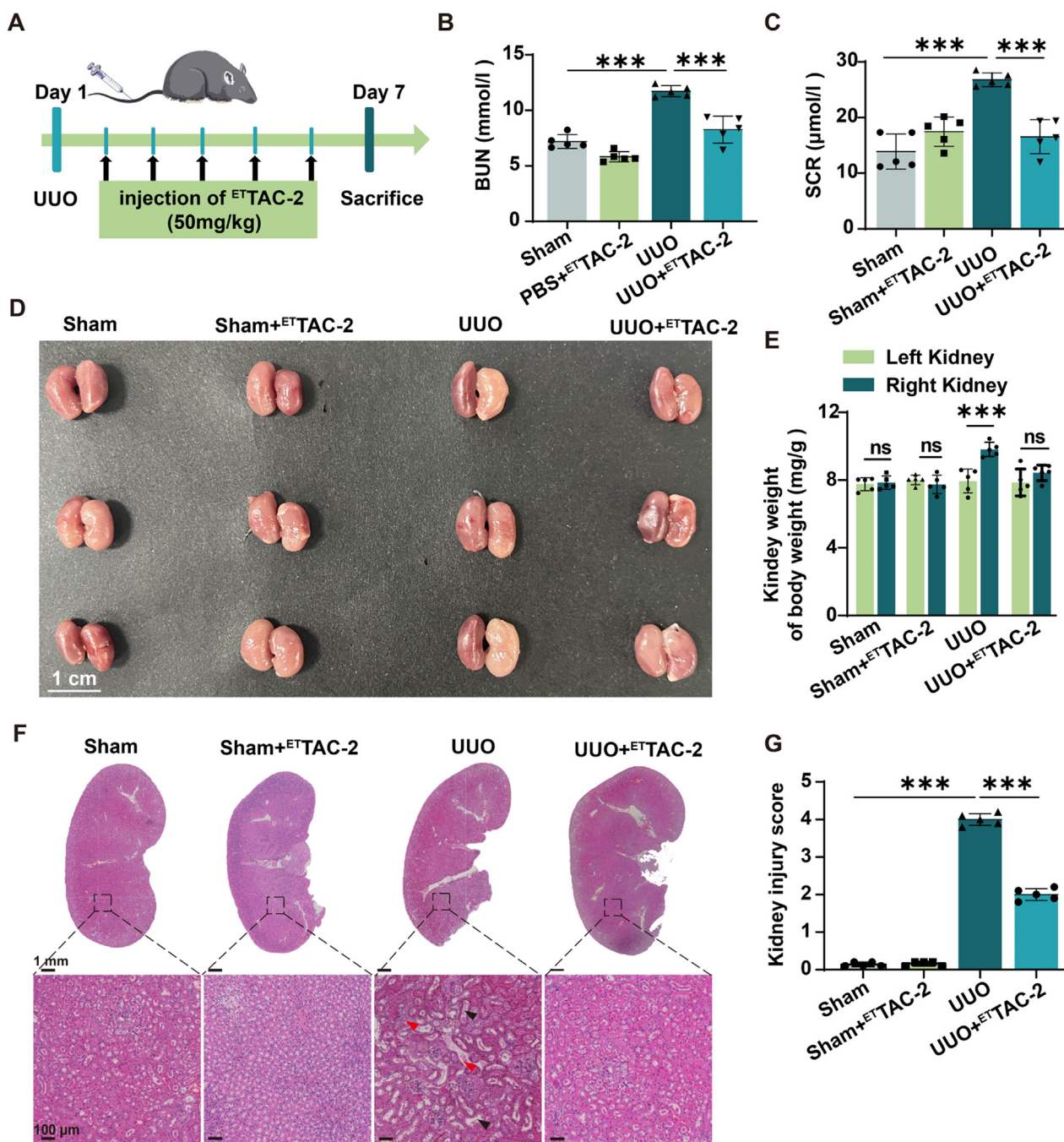
Fig. 4 – ᴱᵀTAC-2 protects renal function post-UUO *in vivo*. (A) Schematic illustration of treatment schedule. (B) BUN and (C) SCR levels of mice with different treatments ($n = 5$). (D) Representative images of kidneys *ex vivo* from mice with different treatments. (E) The quantitative analysis of the ratio of kidney weight to body weight of mice from different treatments ($n = 5$). (F) Representative images of H&E staining and (G) corresponding kidney injury score of kidney tissues from mice with different treatments ($n = 5$). Data are shown as mean ± SD; ***$P < 0.001$; ns, no significance $P > 0.05$ when compared between indicated groups by 2-way analysis of variance with a Tukey post hoc test.

in LRG1 expression in the kidneys of mice subjected to UUO. ᴱᵀTAC-2 treatment led to a 46.9% decrease in LRG1 overexpressed in these kidneys post-UUO. Additionally, Western blot analysis quantitatively confirmed ᴱᵀTAC-2′s influence on LRG1 expression in these samples. Data from Fig. 6C and D indicated a 62.9% reduction in LRG1 levels post-UUO treatment with ᴱᵀTAC-2.

Subsequently, we evaluated the activation of the TGF-β-Smad3 signaling pathway in mouse kidneys following ᴱᵀTAC-2 treatment. Fig. 6E illustrated a significant increase in the pink fluorescent signal of phosphorylated Smad3 in kidney cells following UUO, alongside pronounced tubular dilation. Treatment with ᴱᵀTAC-2 led to a marked reduction in these pink fluorescent signals and a notable improvement in tubular
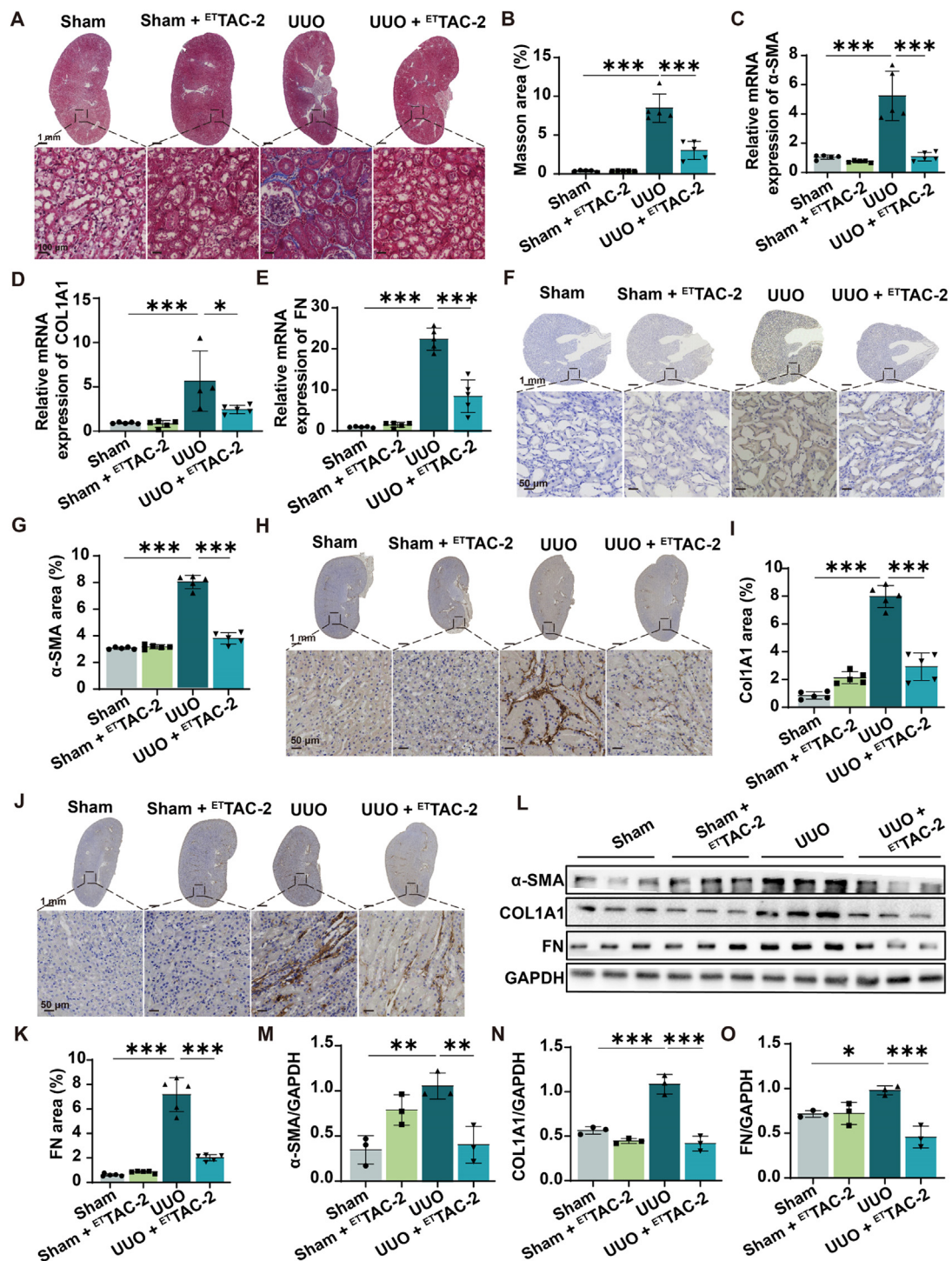
Fig. 5 – ᴱᵀTAC-2 alleviates renal fibrosis of mice *in vivo*. (A) Representative Masson staining images and (B) corresponding semi-quantitative analysis of deposited collagen in kidneys from mice with different treatments ($n = 5$). (C-E) Relative mRNA levels of α-SMA, collagen1A1, and fibronectin in kidney tissues from mice with different treatments ($n = 5$). (F-K) Representative images and corresponding semi-quantitative analysis of α-SMA, collagen1A1, and fibronectin expressed in kidney tissues from mice with different treatments ($n = 5$). (L-O) Representative western blot images of α-SMA, collagen1A1, and fibronectin expressed in kidney tissues with different treatments ($n = 3$). Data are shown as mean ± SD; *$P < 0.05$; **$P < 0.01$; ***$P < 0.001$ when compared between indicated groups by two-way analysis of variance with a Tukey post hoc test.

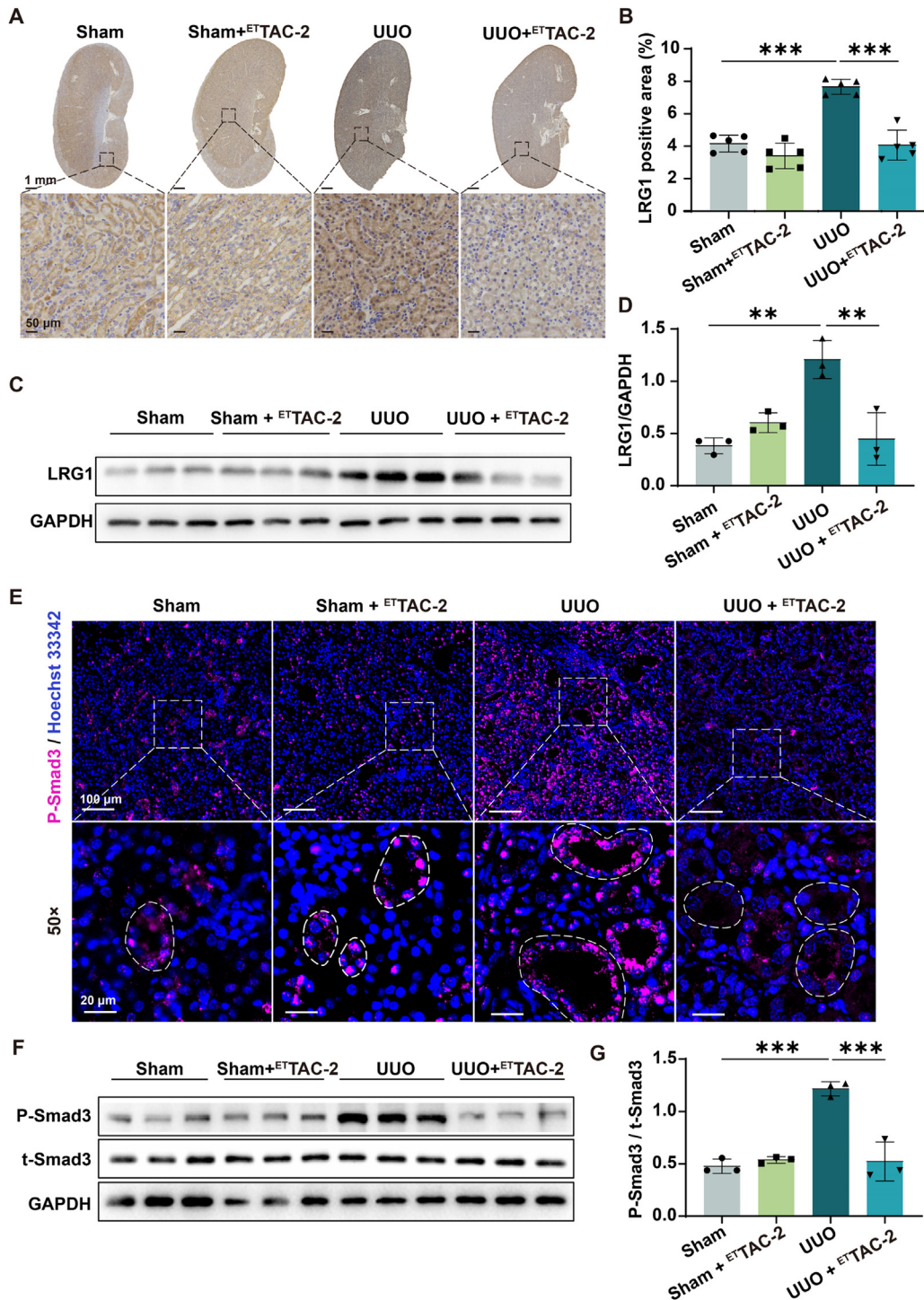**Fig. 6 – Mechanism study of ETTAC-2 mediated anti-fibrosis *in vivo*. (A)** Representative immunohistochemical staining images and **(B)** corresponding semi-quantitative analysis of LRG1 in kidney tissues from mice with different treatments. *n* = 5 Per group. **(C)** Western blot images and **(D)** corresponding quantitative analysis of LRG1 expressed in kidney tissues of mice with different treatments. *n* = 3 Per group. **(E)** Representative immunofluorescence staining of P-Smad3 expressed in kidney tissues from mice with different treatments. **(F)** Western blot images and **(G)** corresponding quantitative analysis of t-Smad3 and P-Smad3 expressed in kidney tissues of mice with different treatments. *n* = 3 Per group. Data are shown as mean ± s. d; **$P < 0.01$; ***$P < 0.001$ when compared between indicated groups by two-way analysis of variance with a Tukey post hoc test.

structure. Additionally, Western blot analysis was utilized to quantitatively assess alternation in Smad3 phosphorylation. As illustrated in Fig. 6F and 6G, phosphorylated Smad3 levels increased significantly post-UUO but decreased by 57.1% after [ET]TAC-2 treatment. These results corroborated with our cellular-level mechanistic studies, highlighting [ET]TAC-2′s role in attenuating mouse kidney fibrosis predominantly by degrading LRG1 and subsequently inhibiting the TGF-β-Smad3 signaling pathway.

3.8. Biosafety evaluation of [ET]TAC-2 in vivo

Considering the versatile role of LRG1 in physiological processes, the biosafety of [ET]TAC-2-based therapy for renal fibrosis was evaluated. Monitoring of body weight of mice during the treatment period revealed that [ET]TAC-2 had no significant impact on their body weight (Fig. S10). Post-treatment, major organs (including heart, liver, spleen, and lungs) were collected for morphological examination. As shown in Fig. S11, [ET]TAC-2 treatment did not induce notable morphological alterations in these organs. Collectively, these results suggest that [ET]TAC-2-mediated anti-fibrotic therapy is biologically safe.

4.   Conclusion

Considering the pivotal role of LRG1 in advancing renal fibrosis and the recently identified LRG1-targeting peptide, we have engineered a novel proteolysis-targeted chimera, [ET]TAC-2, with the explicit purpose of degrading LRG1 to alleviate renal fibrosis. Upon internalization by fibrotic renal cells, [ET]TAC-2 initiates the ubiquitination and subsequent degradation of LRG1, leading to a decline of the extracellular secretion of LRG1. This decrease effectively dampens the activation of the TGF-β-Smad3 signaling pathway, thereby suppressing extracellular matrix production, and markedly inhibiting the progression of renal fibrosis. Our findings, corroborated through both in vitro and in vivo studies, endorse LRG1 as a viable therapeutic target and position [ET]TAC-2 as a groundbreaking tool for targeted therapy against renal fibrosis.

Conflicts of interest

The authors report no conflicts of interest. The authors alone are responsible for the content and writing of this article.

Acknowledgments

Supplementary materials

Supplementary material associated with this article can be found, in the online version, at doi:10.1016/j.ajps.2024.100941.

REFERENCES

[1] Liu KD, Goldstein SL, Vijayan A, Parikh CR, Kashani K, Okusa MD, et al. AKI! now initiative: recommendations for awareness, recognition, and management of AKI. Clin J Am Soc Nephrol 2020;15(12):1838–47.

[2] Ruiz-Ortega M, Rayego-Mateos S, Lamas S, Ortiz A, Rodrigues-Diez RR. Targeting the progression of chronic kidney disease. Nat Rev Nephrol 2020;16(5):269–88.

[3] Lopez-Novoa JM, Martinez-Salgado C, Rodriguez-Pena AB, Lopez-Hernandez FJ. Common pathophysiological mechanisms of chronic kidney disease: therapeutic perspectives. Pharmacol Ther 2010;128(1):61–81.

[4] Zhao X, Kwan JYY, Yip K, Liu PP, Liu FF. Targeting metabolic dysregulation for fibrosis therapy. Nat Rev Drug Discov 2020;19(1):57–75.

[5] Zhu X, Zhao Y, Liu Y, Shi W, Yang J, Liu Z, et al. Macrophages release IL11-containing filopodial tip vesicles and contribute to renal interstitial inflammation. Cell Commun Signal 2023;21(1):293.

[6] Meng XM, Nikolic-Paterson DJ, Lan HY. TGF-β: the master regulator of fibrosis. Nat Rev Nephrol 2016;12(6):325–38.

[7] Isaka Y. Targeting TGF-β signaling in kidney fibrosis. Int J Mol Sci 2018;19(9):2532.

[8] Yang Q, Xie RJ, Yang T, Fang L, Han B, Zhang GZ, et al. Transforming growth factor-beta1 and Smad4 signaling pathway down-regulates renal extracellular matrix degradation in diabetic rats. Chin Med Sci J 2007;22(4):243–9.

[9] Chevalier RL, Forbes MS, Thornhill BA. Ureteral obstruction as a model of renal interstitial fibrosis and obstructive nephropathy. Kidney Int 2009;75(11):1145–52.

[10] Hu HH, Chen DQ, Wang YN, Feng YL, Cao G, Vaziri ND, et al. New insights into TGF-β/Smad signaling in tissue fibrosis. Chem Biol Interact 2018;292:76–83.

[11] Massagué J, Sheppard D. TGF-β signaling in health and disease. Cell 2023;186(19):4007–37.

[12] Yadav H, Quijano C, Kamaraju AK, Gavrilova O, Malek R, Chen W, et al. Protection from obesity and diabetes by blockade of TGF-β/Smad3 signaling. Cell Metab 2011;14(1):67–79.

[13] Lan HY. Diverse roles of TGF-β/Smads in renal fibrosis and inflammation. Int J Biol Sci 2011;7(7):1056–67.

[14] Wu W, Wang X, Yu X, Lan HY. Smad3 signatures in renal inflammation and fibrosis. Int J Biol Sci 2022;18(7):2795–806.

[15] Secker GA, Shortt AJ, Sampson E, Schwarz QP, Schultz GS, Daniels JT. TGFbeta stimulated re-epithelialization is regulated by CTGF and Ras/MEK/ERK signaling. Exp Cell Res 2008;314(1):131–42.

[16] Chen YG. Endocytic regulation of TGF-beta signaling. Cell Res 2009;19(1):58–70.

[17] Kudlow JE, Bjorge JD. TGF alpha in normal physiology. Semin Cancer Biol 1990;1(4):293–302.

[18] Brachmann R, Lindquist PB, Nagashima M, Kohr W, Lipari T, Napier M, et al. Transmembrane TGF-alpha precursors activate EGF/TGF-alpha receptors. Cell 1989;56(4):691–700.

15

[19] Arcidiacono MV, Cozzolin M, Spiegel N, Tokumoto M, Yang J, Lu Y, et al. Activator protein 2alpha mediates parathyroid TGF-alpha self-induction in secondary hyperparathyroidism. J Am Soc Nephrol 2008;19(10):1919–28.

[20] Camilli C, Hoeh AE, De Rossi G, Moss SE, Greenwood J. LRG1: an emerging player in disease pathogenesis. J Biomed Sci 2022;29(1):6.

[21] Liu TT, Luo R, Yang Y, Cheng YC, Chang D, Dai W, et al. LRG1 mitigates renal interstitial fibrosis through alleviating capillary rarefaction and Inhibiting inflammatory and pro-fibrotic cytokines. Am J Nephrol 2021;52(3):228–38.

[22] Hong Q, Cai H, Zhang L, Li Z, Zhong F, Ni Z, et al. Modulation of transforming growth factor-β-induced kidney fibrosis by leucine-rich α-2 glycoprotein-1. Kidney Int 2022;101(2):299–314.

[23] Wang C, Zheng C, Wang H, Zhang L, Liu Z, Xu P. The state of the art of PROTAC technologies for drug discovery. Eur J Med Chem 2022;235:114290.

[24] Békés M, Langley DR, Crews CM. PROTAC targeted protein degraders: the past is prologue. Nat Rev Drug Discov 2022;21(3):181–200.

[25] Li X, Song Y. Proteolysis-targeting chimera (PROTAC) for targeted protein degradation and cancer therapy. J Hematol Oncol 2020;13(1):50.

[26] Xiong Y, Zhong Y, Yim H, Yang X, Park KS, Xie L, et al. Bridged proteolysis targeting chimera (PROTAC) enables degradation of undruggable targets. J Am Chem Soc 2022;144(49):22622–32.

[27] Dragovich PS. Degrader-antibody conjugates. Chem Soc Rev 2022;51(10):3886–97.

[28] Guenette RG, Yang SW, Min J, Pei B, Potts PR. Target and tissue selectivity of PROTAC degraders. Chem Soc Rev 2022;51(14):5740–56.

[29] Chen MD, Zhu AY, Zhu FR, Lei ZW, Huang T, Du SN, et al. Identification of LRG1 targeting peptide and its application in targeted imaging for breast cancer. Nano Res 2023. doi:10.1007/s12274-023-6268-8.